
Article:
Bhattacharya, P. and Siegmund, T.H. (2012) A Canonical Biomechanical Vocal Fold Model. Journal of Voice, 26 (5). pp. 535-547. ISSN: 0892-1997

https://doi.org/10.1016/j.jvoice.2011.09.001

A Canonical Biomechanical Vocal Fold Model

Pinaki Bhattacharya[a], Thomas H. Siegmund[a]

[a]School of Mechanical Engineering, Purdue University, West Lafayette, IN 47906 USA

Summary: The present paper aimed at constructing a canonical geometry of the human vocal fold (VF) from subject-specific image-slice data. A computer-aided-design approach automated the model construction. A subject-specific geometry available in literature, three abstractions (which successively diminished in geometric detail) derived from it, and a widely-used quasi two-dimensional VF model geometry were used to create computational models. The first three natural frequencies of the models were used to characterize their mechanical response. These frequencies were determined for a representative range of tissue biomechanical properties, accounting for underlying VF histology. Compared to the subject-specific geometry model (baseline), a higher degree of abstraction was found to always correspond to a larger deviation in model frequency (up to 50% in the relevant range of tissue biomechanical properties). The model we deemed canonical was optimally abstracted, in that it significantly simplified the VF geometry compared to the baseline geometry, but can be recalibrated in a consistent manner to match the baseline response. Models providing only a marginally higher degree abstraction were found to have significant deviation in predicted frequency response. The quasi two-dimensional model presented an extreme situation: it could not be recalibrated for its frequency response to match the subject-specific model. This deficiency was attributed to complex support conditions at anterior-posterior extremeties of the VFs, accentuated by further issues introduced through the tissue biomechanical properties. In creating canonical models by leveraging advances in clinical imaging techniques, the automated design procedure makes VF modeling based on subject-specific geometry more realizable.

Key Words: vocal fold, geometric model, tissue biomechanical properties, eigenfrequencies

INTRODUCTION

The pair of vibrating vocal folds (VFs)[†] within the larynx are important components relevant to the production of voice. The need to understand the phonation mechanism and biomechanical factors affecting voice health drives research using VF models. Figure 1 shows the anatomy of a typical pair of VFs situated in the larynx. In this paper, we focus on the VFs system comprising the lamina propria, vocal fold ligament and underlying thyro-arytenoid muscle, bounded by the hard arytenoid and thyroid cartilages. The system boundary is depicted in figure 1. We aim to develop rules for VF model construction such that VF biomechanical response agrees with that of a corresponding subject-

[†]Table 1 summarizes all symbols and definitions.

specific VF. A subject-specific VF will have the features shown in figure 1 in general, along with details particular to itself. The envisaged model is canonical in that any further abstraction in geometry, with respect to that of the subject-specific VF, will cause its mechanical response to deviate from the subject response by more than a specified tolerance. This model can then be used to understand and predict phonation and voice health characteristics of the subject-specific VF.

Application of continuum mechanics principles in the analysis of voice processes has received significant attention in the past. Examples include studies of the fundamental processes of phonation mechanism [1,2], the modeling of continuum response using advanced constitutive theories [3,4,5], the determination of mechanical stress within the folds [6], the computations of impact pressures at contacting glottal surfaces during vibration [7,8,9]. In a continuum mechanics setting, accurate geometrical representation of the system of interest is essential to model a problem. The geometric description of vocal folds in continuum mechanics studies commonly are based on significant abstraction of the anatomical and geometrical features. We hypothesize that the degree of model abstraction will influence the predicted biomechanical response of the VFs, and that appropriate rules of model abstractions can be developed such that the relevant mechanisms underlying phonation can effectively be analyzed and described. The desire to obtain an abstraction of subject-specific anatomical features of the VFs is driven by advantanges in ease of modeling and analysis, but also by the desire to extract fundamental insight by eliminating confounding factors.

An underlying principle in the abstraction process is that, to a specified order of accuracy, the mechanism being studied is not affected by the geometric features that are absent in the abstracted model. Therefore, unless both the original and the abstracted structure are actually analyzed for their relevant behavior, and the property to be studied (the fundamental frequency, a magnitude of stress, etc.) is shown to be insensitive to the features removed – the results obtained from the model are not relevant.

In this paper we present a method that utilizes slice-by-slice section images of the three-dimensional VF to develop subject-specific models for phonation. Such image information is available from magnetic resonance imaging (MRI), computed tomography (CT), but also from more traditional methods based on castings like those obtained by Šidlof et al. [10] In particular, MRI data of VFs is the most detailed in-vivo anatomical information available, and provides [11,12,13] superior image results when compared to CT technology. Continuum mechanics analysis of a VF model created based on MRI data [14] demonstrated the importance of careful model abstraction. These authors found significant differences in the self-oscillation response of a model based on MRI data when compared to mechanisms predicted [6,7,15,16,17] from the commonly employed M5 model [18].

The M5 model was developed as a canonical model for the analysis of glottal air flow around the VFs, but was subsequently also used in continuum mechanics analysis of the VFs themselves. Its geometry is a specification of the planar curve lying at the intersection of the medial surface and the mid-coronal section of the VF. This specification was a development over previous two-dimesional modeling efforts of Ishizaka and Flanagan [19], Scherer et al. [20], van den Berg et al. [21], Gauffin et al. [22] As only air flow was of interest, the model does not account for underlying histology of the VF vol-

ume, and due to its 2D character leaves the lateral extent and anterior–posterior (*ap*) description of the glottal surface as free parameters. Significant computational research effort [1,23,18,24,25] has been directed at the M5 and similar other 2D geometries. Simple extensions of this model into 3D space [26,27,17,18,24] have been used to conduct computational and experimental research. The limitations of the M5 model were also recognized and extensions of the original model were defined, [28,29,30,7] emerging from a need to explain particular experimental observations absent in a model of simpler geometric definition.

In contrast to the path of gradual sophistication of the M5 canonical model, we believe that a more robust approach to model definition is to conduct sensitivity studies on gradual simplifications of a subject-specific VF geometry. Such an approach is considered in the present study, and in addition, the interaction of VF model geometry with tissue biomechanical properties was also considered.

The work documented in Pickup and Thomson [14] partially follows the same direction of approach as it appears to be the first attempt at sensitivity analysis with a subject-specific geometry as the baseline. In particular it was observed in Pickup and Thomson [14] that mucosal-waves were possible only in an MRI-motivated geometric model and not in the canonical model. However, in a flow-structure-interaction analysis as considered in Pickup and Thomson [14] VFs undergo very highly nonlinear deformation. Thus it is difficult to relate difference in deformation characteristics to differences in geometry. In the present paper, instead, we seek to investigate a more basic feature of the VF model, namely the natural frequency. This allows for a broader range of geometric abstraction level and consideration of the interaction with the tissue's biomechanical properties. Although MR imaging of human VFs is able to differentiate hard cartilages in the larynx from soft tissue [31,12,13,32], we are unaware of its capability to recognize and distinguish underlying tissue histology. Therefore, an assumed cover thickness is used to define an identical body-cover partition in all the models.

In the analysis we focus on the first three natural modes of vibration as these were shown by Zhang et al. [33] to account for 99% of the energy at the onset of self-oscillation.

A rational modeling methodology is presented, that goes from highly geometrically accurate models to subsequently abstracted ones in a graduated manner. Along this path, removal of each feature can be tested for sensitivity to the object of analysis. We demonstrate that knowledge of tissue properties is crucial to capture the correct frequency response even under conditions of accurate geometric representation.

The structure of this paper is as follows. In the following section, we present a general and versatile formulation which enables the creation of geometric model of a particular human VF configuration. The versatility of the formulation – implemented in a commercial computer-aided design (CAD) software package – is further demonstrated by incorporating geometric abstractions. The formulation is exercised by considering a particular subject-specific VF configuration as previously documented in the literature [10]. Geometrically abstracted models based on the same subject-specific data are constructed.

It is important that the analysis model capture important features of the histological structure present in the tissue. In particular, for VFs we follow the body-cover theory, which is used to represent the histology of the

VF tissue. It separates the VF into a stiffer and isotropic interior part (body) and a more compliant anisotropic domain (cover) near the surface[3]. In the context of model development, a partitioning strategy allowing for body-cover regions in the model geometry is developed. Farley [34] studied the effect of activation of various ligament and muscle structures in the larynx on the frequency of phonation. Activation levels corresponded to tension within these structures. The effect of muscle activation is analyzed herein by controlling the stiffness of the body region. Transverse anisotropy of the cover region is modeled using a consistent micromechanical model.

FE analysis is conducted to determine the first three natural frequencies of the models in dependence of tissue properties. Variation in levels of body-cover heterogeneity and anisotropy of tissue biomechanical properties are considered in isolation as well as in combination. Our results demonstrate the effect of tissue properties on eigenfrequency. In the light of these results, we conclude by pointing to future research required to create effective but accurate computational models of VFs.

METHODS

Vocal fold geometry

Image-slice based methods

A method is described by which digitized image-slice data representing the 3D image of the VF configuration can be converted into a 3D continuum model. The first step is to define a coordinate system and origin. The coordinate axes are aligned with respect to established anatomical planes. Conventions followed in previous research[35,36] assume the cricoid cartilage (CC) to be symmetric about the mid-saggital plane. Therefore, using image-slice data for CC, we define the mid-saggital plane as the one coinciding with its plane of symmetry. Similarly, the mid-coronal plane is identified as that located midway between the anterior-commissure and the line joining the left and right crico-arytenoid joints. The origin of the coordinate system is located arbitrarily on the intersection of the mid-coronal and mid-saggital planes. The x-axis increases in the superior direction, the y-axis is normal to the saggital planes and positive y-values correspond to the right VF. A right-hand coordinate system is then determined by fixing the z-axis such that it increases going from posterior to anterior, and is perpendicular to all coronal planes.

We assume that images of M coronal planes (parallel to each other) are available. Each coronal plane corresponds to $z = z^{(i)}, (i = 1 \dots M)$. Each of the M images is individually digitized to obtain N points at equal intervals along the profile. In the inferior–superior (is) direction geometric features of human VFs change substantially over a characteristic distance of 5 mm, and the characteristic radius of curvature of the glottal surface is of the order of 1 mm[18]. Therefore considering $N = 20$ results in a reasonably resolved profile. We denote the coordinates of these points by the label $P_j^{(i)}\Big|_{L,R} \equiv (x_j^{(i)}, y_j^{(i)}\Big|_{L,R}, z^{(i)})$ where $j = 1 \dots N$ and subscripts L and R denote points on the left and right VF respectively. The outer boundary vocal tract is assumed to be cylindrical, and its diameter H is chosen such that it satisfies

$$H > \sqrt{\left[y_j^{(i)}\Big|_{L,R}\right]^2 + [z^{(i)})]^2} \qquad \forall P_j^{(i)}. \tag{1}$$

Two circles, of diameter H, centered at $(x_{\min}, 0, 0)$ and $(x_{\max}, 0, 0)$ are used to form the closed curves S_0 and S_{N+1} that mark, respectively, the inferior and superior extremeties of the model. Therefore the locations $x_{\min}$

and $x_{\max}$ along the inferior–superior axis satisfy

$$x_{\min} < \inf_{P_j^{(i)}} x_j^{(i)}, \qquad x_{\max} > \sup_{P_j^{(i)}} x_j^{(i)}. \tag{2}$$

The procedure for creating the model geometry is shown in figure 2. A software implementation, by means of a Python script in a computational code, i.e. ABAQUS/CAE, was employed to code the process. This script is available from the authors upon request. Subsequently, the subject-specific geometric model incorporating subject-specific anatomical feature geometry is referred to as model SS.

The M5 model

The M5 model geometry as of Scherer et al. [18] is considered for comparison. As mentioned earlier, the M5 model in particular has seen widespread use in both numerical and experimental modeling. The abstraction from subject-specific geometry to a quasi-2D M5 (extruded geometry) will cause an error of some magnitude in the model response. If this error is not significant, finer alterations on the M5 model to obtain other 2D specifications can be justified, in order to fine tune the model response. Otherwise, the choice between an extruded M5 model or any other extruded model is moot. Thereby, comparing with the M5 model here also serves as a substitute for other 2D or extruded geometry formulations.

In particular, the M5 is defined as described in figure 3 (a). In models based on the 2D M5 geometry, the left and right VFs are disjoint, and symmetry about the mid-saggital plane is assumed. The 2D profile does not specify a VF depth ($D/2$, medial–lateral extent) and D is a free parameter in the model. In figure 3 (a), it can be seen that horizontal line forming the superior edge and the slanted line leading up to the glottal entrance can be extended to form a VF of any given depth. In Scherer et al. [18], physical replicas were constructed with $D/2 = 11.48$ mm. Note that the subglottal surface makes an angle of 40° with the horizontal.

Another free parameter of the M5 profile is the glottal angle ψ. The profile was originally intended to be used in static glottal models where the flow field around the geometry was the object of investigation. The parameter ψ accounted for the dynamic glottal angle that followed the inferior-superior motion of the VFs during phonation. In models capable of moving and/or deforming, setting $\psi = 0°$ suffices, because the glottal angle changes once motion commences. In Scherer et al. [18], the physical replicas used a range of values for ψ to analyse its effect on flow characteristics.

Being a 2D formulation, the length (ap-extent) of the VF is also unspecified in the M5 model. Beginning with Alipour et al. [28], who set the foundation for FE modeling of VFs, 3D models based on the M5 profile typically [8,29,37,38,27] identified the ap-extent of the model with the ap-extent of the glottal orifice. In Scherer et al. [18], for instance, physical replicas of the VFs had a constant length $L = 12.0$ mm. The 3D model was created by extruding the 2D M5 profile through this length.

For the present study we consider M5 geometry as of figure 3 (b). This profile of the M5 model considers $\psi = 0°$ and is extended upto the outer tracheal wall by setting $D = H - d_g$.

Abstracted vocal fold geometries

Departing from the subject-specific VF geometry, the procedure in figure 2 allows for the creation of models with geometric abstractions made at various levels. An example of this process is present in the following. The ap variation of the M coronal images used to construct

the subject-specific model SS are simplified in a process in which the mid-coronal features $(x_j^{(M/2)}, y_j^{(M/2)}, z^{(M/2)})$ are retained from SS. Here $M/2$ is the index of the mid-coronal plane. The M coronal images are replaced by the point-set

$$\bar{P}_j^{(i)}\Big|_{L,R} = \left(\bar{x}_j^{(i)}, \bar{y}_j^{(i)}\Big|_{L,R}, \bar{z}_j^{(i)}\right), \tag{3}$$

where

$$\begin{aligned} \bar{x}_j^{(i)} &= x_j^{(M/2)}, \\ \bar{y}_j^{(i)}\Big|_{L,R} &= \pm a\left[1 - \left(\frac{\bar{z}_j^{(i)}}{b}\right)^{\frac{2}{k}}\right]^{1/2}, \\ \text{and} \quad \bar{z}_j^{(i)} &= z_j^{(i)}. \end{aligned} \tag{4}$$

Thereby, a, b and k are functions of $\bar{x}_j^{(i)}$, and H is the maximum width of the glottal tract. This definition ensures the glottal opening appears to be smooth and rounded when viewed from the superior aspect. The parameter

$$k = k(\bar{x}_j^{(i)}) = \frac{1}{4} + \frac{3}{4}\left(\frac{a - d_g/2}{H/2 - d_g/2}\right)^{1/2}, \tag{5}$$

ranges between 0.25 and 1.0, and controls the curvature at the anterior and posterior ends of the glottal opening along the inferior-superior direction. Note that the case $k \to 0$ approaches a rectangle of dimensions $2b \times 2a$ and the case $k = 1$ corresponds to an ellipse inscribed in this rectangle. Thereby, the shape of the glottal opening is more rounded near the glottal orifice compared to an ellipse of identical axis measures.

The glottal half-width at the mid-coronal section is

$$a(\bar{x}_j^{(i)}) = \frac{1}{2}\left(\bar{y}_j^{(i)}\Big|_R - \bar{y}_j^{(i)}\Big|_L\right), \tag{6}$$

and defines the semi-minor axis of the glottal tract cross section. The ap extent, identical to the semi-major axis, is

$$b(\bar{x}_j^{(i)}) = H/2 - w\left(\frac{H/2 - a}{H/2 - d_g/2}\right), \tag{7}$$

which allows for a depth w at the anterior and posterior ends of the folds near the glottal orifice. This model defined by these parameters is henceforth called R0. Its mid-coronal geometry is identical to that of the subject-specific model SS, figure 3 (b).

Additional VF geometries are created by merging the shape information of the R0 model with the M5 model. A model R2 is created by replacing the mid-coronal profile in model R0 by the particular section shape of the M5 model profile considered in the previous section and depicted in figure 3 (b). The 3D configuration is then created by repeating the procedure outlined in the previous paragraph.

Model R1 is an intermediate configuration between model R0 and model R2. Figure 3 (b) shows that in R0, the surface inferior to the glottal entrance (or the subglottal surface) makes an angle of approximately 53° with the horizontal, compared to 40° in model R2. Model R1 differs from model R2 only in the region inferior to the glottal-entrance, where it closely follows model R0. The rest of the procedure for creating model R1 is identical to that of model R2. We also consider a model in which the mid-coronal section of model R1 is extruded through a given length L to create the 3D model M5R1.

Partitioning into body-cover domains

In Hirano [39], it was shown that the VF volume is not homogeneous. Following the notation of the body-cover model, distinct histology is attributed to two distinct regions of the VF. The outer, compliant cover layer, is thereby distinguished from the body across an internal boundary.

On the mid-coronal plane a segmentation into the body and cover is defined by specification of an inter-

nal partition line, as shown in figure 4. This partition line is swept along an arc in the transverse plane to obtain the interface between the cover and body regions. The radius of the arc is R and the distance of the center of the arc from the VF axis is $C = R - H$. In the absence of subject-specific histological data, R is retained as a free model parameter. Its numerical value is chosen such that the thickness of the cover at all coronal sections remains $\sim O(t)$. The tissue properties of the two layers are identified by subscripts b and c referring to body and cover respectively. The dotted line shows the body-cover partition interface.

Specific model parameters

In Šidlof et al. [10] a casting method was used to obtain the geometry of the VFs of a 72-year old female subject. Eight coronal sections ($M = 8$), each 1 mm apart, were considered (see figure 5). The data[10] did not include information on the cricoid cartilage and joint locations. Therefore the mid-saggital plane is defined such that the minimum distance between this plane and the left and right profile on each coronal plane is on average zero. This model is referred to as model SS.

To create the models R0, R1 and R2, the mid-coronal section of model SS is required. Image-slices in figure 5 are taken at a series of equispaced locations along the anterior-posterior direction. Therefore, slices at $z = 7.5$ mm and $z = 8.5$ mm (Šidlof et al. [10] coordinates) are obvious choices for the mid-coronal section. The plane with index $z = 7.5$ mm (Šidlof et al. [10] coordinates) was chosen as the mid-coronal plane. The models SS, R0, R1 and R2 are meshed using continuum 3D 4-noded tetrahedral elements (C3D4) by a free mesh-generation technique. The global element edge length L_{elem} is set to 0.300 mm, with the curvature-control and size factors set to 0.030 and 0.100 respectively. Interior elements are allowed to increase in size. For the M5R1 model, $L_{elem} = 0.500$ mm, and the curvature-control and size factors are same as for the subject-specific models. It is meshed with 3D 8-noded quadrilateral elements (C3D8). The sweep technique with the advancing-front algorithm is used to generate the mesh. The number of elements generated depends on the length of the model considered. Table 2 summarizes the model data. Note that the range of vertical axis in figure 5 is ≈ 15 mm. In order to accommodate the images and smoothly merge them into a cylindrical tracheal wall of diameter H, the numerical value of H is specified to be somewhat larger. The image slices corresponding to anterior and posterior extremeties in figure 5 show the left and right VFs to be separate by $\gtrsim 1$ mm. Thereby, the VFs needed to be extended by $w \gtrsim 1$ mm in both anterior and posterior directions to merge them smoothly without creating sharp corners. The choice of cover thickness $t \sim 2$ mm (figure 3 b) agrees with earlier measurements. For example, Hirano et al. [40] observed that the epithelial layer, and the superficial and intermediate layers of the lamina propria, which together constitute the cover, are 1.0–1.5 mm thick. The radius R of the arc defining the body-cover partitioning ensures that the cover thickness varies between 0.985 mm and 2.00 mm at any location. With respect to the average value of the H parameter, each geometric parameter deviates from its mean by no more than 7.6%. These small differences arise out of human intervention required in creating the models.

Tissue biomechanical properties

The mass density $\rho_{b,c} = 1070$ kg/m^3 of the body and cover regions is taken to be close to the density of water, the major constituent of biological tissue. Similar

values are reported in Titze [41] for the thyro-arytenoid muscle which makes up the bulk of the body. In a linear perturbation analysis, as conducted in this paper, strains are assumed to be infinitesimal. Under this assumption, considering non-linear stress-strain response for the tissue does not lead to any further insight. The cover region is postulated to be transversely anisotropic[3], with stiffness in ap-direction being higher than in the isotropic coronal plane perpendicular to it. In the following, subscripts *ml* (medial–lateral) and is identify two mutually perpendicular directions in the coronal plane. We use a consistent micromechanical model (Daniel and Ishai [42], ch. 3) to obtain the elastic constants of a transversely isotropic elastic constitutive law for the cover region. To this effect, the cover region is assumed to comprise two constituents: the load-bearing collagen fibers (oriented along the ap-direction) and the underlying extra cellular matrix. From measurements on excised larynges[4] we estimate $E_{ap} \sim 6$ kPa. The matrix is considered to be close to incompressible, $\nu_m = 0.490$. The Poisson's ratio of the fiber is considered to be $\nu_f = 0.300$ and its volume fraction to be 30%. To complete the model, we need to specify the elastic moduli of the fibers and the matrix components, i.e. E_f and E_m respectively. Let us define the ratio between the elastic moduli in the ap-direction to that in any direction in the coronal plane (for e.g. *ml* here)

$$\chi \equiv E_{ap}/E_{ml}, \tag{8}$$

as a measure of the degree of anisotropy in the material. The two parameters E_f and E_m can be uniquely specified to obtain target values of χ and $E_{c,ap}$. Table 3 gives elastic constants obtained for the cover derived from the micromechanical model for the four values of $\chi = 1.00$ (isotropic), 2.00, 5.00 and 10.0. Kelleher et al. [3] found that the ligament can have anisotropy as high as $\chi \sim 50$. Therefore the values we consider here are well within the expected range.

In Oestreicher [43] it was argued that soft biological tissue like the VFs are typically almost incompressible, because they comprise mostly of water, which is incompressible under standard temperature and pressure conditions. Thereby we consider the body to be close to incompressible and fix $\nu_b = 0.450$. To simulate stiffening of the body region, we consider various values of $h = E_b/E_{c,ap}$, by increasing E_b and keeping $E_{c,ap}$ fixed.

The following cases are considered for the subject-specific models presented in the preceeding section. Firstly, we simulate a homogeneous isotropic VF by setting $E_b = E_{c,ap} = 6.00$ kPa and $\chi = 1.00$. The effect of muscle activation is analyzed by increasing E_b, such that $h = 2.00, 4.00$ and 8.00. Previous studies[44,45] report that stresses in an active muscle can be an order of magnitude higher than passive muscle. Therefore the values of h considered here should be taken to be indicative. The effect of anisotropy is investigated with $h = 1.00$ and setting cover properties from table 3 corresponding to $\chi = 2.00, 5.00$ and 10.0. To investigate the combined effect of muscular activation and cover anisotropy, we consider the following scenarios. On one hand, we fix $h = 4.00$ ($E_b = 24.0$ kPa) and $E_{c,ap} = 6.00$ kPa and vary the level of anisotropy in the cover ($\chi = 2.00, 5.00$ and 10.0). On the other hand, we fix $\chi = 5.00$ and $E_{c,ap} = 6.00$ kPa, and vary the level of muscle activation by increasing E_b such that $h = 2.00, 4.00$ and 8.00. The case ($h = 4.00, \chi = 5.00$) is encountered along both lines of variation.

EIGENFREQUENCY ANALYSIS

We undertake an eigenfrequency analysis to investigate the influence of VF geometry and biomechanical properties on the frequency response of the VFs. Boundary conditions imposed on the FE models are as follows. The tracheal walls are much stiffer compared to the VFs, and are assumed to be rigid in this study. To simulate this, we constrain all degrees of freedom of the outer surface of subject-specific models. For model M5R1, this means that the ap end-surfaces and the lateral surface are constrained. Also, for this model, considering only one fold suffices because the two folds are disjoint and identical to each other. Following the natural frequency extraction procedure implemented in Abaqus/Standard, an eigenfrequency analysis of an FE model is formulated as solving the following problem

$$\left(-\omega^2 \mathbb{M}^{MN} + \mathbb{K}^{MN}\right) \phi^N = 0, \tag{9}$$

where $\mathbb{M}$ is the mass matrix, $\mathbb{K}$ is the stiffness matrix, ω is the desired eigenfrequency and ϕ^n is the corresponding eigenvector (mode of vibration). Here superscripts M and N denote the degrees of freedom. The Lanczos algorithm is used to solve the problem. We consider the frequencies for the first three natural modes for the models.

RESULTS

We initially consider the models SS, R0, R1 and R3 with isotropic, homogeneous tissue properties, i.e. with no distinction between body and cover. Table 4 shows the first six eigenfrequencies for each of these models. We group the frequency values pairwise, noting their proximity, and calculate averages of paired eigenfrequencies as the effective first, second and third eigenfrequencies. Separations within pairs of eigenfrequencies are due to asymmetries in geometry and mesh with regards to the left and right VF. In the following we refer to the mean of each pair of frequencies as the value corresponding to each mode of vibration, and do not present individual frequency values within each pair.

A mesh independence study was conducted by considering meshes with L_{elem} = 0.300 mm, 0.500 mm, 1.00 mm and 2.00 mm for models SS and R0. The representative cases (h = 1.00, χ = 1.00), (h = 8.00, χ = 5.00) and (h = 4.00, χ = 10.0) were considered. The percentage errors in the first three frequencies are shown in figure 7 in dependence of L_{elem}. Errors are within 6.21% when the L_{elem} is increased from 0.300 mm to 0.500 mm. Therefore, frequencies for models SS, R0, R1 and R2 quoted in this paper correspond to the L_{elem} = 0.300 mm mesh, and are considered to be accurate to within 6.21%. For an M5R1 model with L = 18.0 mm, a similar mesh dependence analysis shows that results are already accurate to within 1.88% when using an L_{elem} = 0.500 mm mesh. Therefore, frequencies for models M5 and M5R1 quoted in this paper correspond to the L_{elem} = 0.500 mm mesh, and are considered to be accurate to within 1.88%.

Figure 8 shows the effect of heterogeneity on the natural frequency response, with the cover being isotropic, for models SS, R0, R1 and R2, as well as for M5R1 models of different lengths. For the range of variation in heterogeneity considered, modal frequencies can change by as much as 50% for all models. However, the frequencies of models SS and R0 are different from each other by at most 2%. This shows that the abstraction is robust to ap variation of geometry. Compared to the baseline model SS, model R1 seems to do better than R2, suggesting an influence of subglottal VF geometry. The former differs from the baseline by at most 10%,

whereas the latter is different by as much as 50% and bearing almost no resemblance to the baseline. Also, note that the ap-extent of the glottal orifice ($H - 2w$) of the subject-specific models (table 2) is on the order of 13.0($\pm$1.20) mm. On the other hand, natural frequencies of the M5R1 model depend on its length L. We observe that the length of the M5R1model required to match the modal response increases as the degree of heterogeneity increases, and this effect is strongest in the case of the first mode.

Figure 8 also compares the frequency, for the models with subject-specific geometry SS and the M5R1 models of different lengths, in dependence of degree of cover anisotropy, with the ratio $h = E_b/E_{c,ap} = 1.00$. Here too, the effect of variation in tissue properties, within each subject-specific model, is seen to be significant. The differences in geometry between the models with subject-specific geometry SS and the other models increases from R0 to R2. The percentage differences are of the same order as in the case of heterogeneity. Another similarity is that increasingly longer M5R1 models are required to match the modal response of subject-specific models at higher anisotropy levels, and this effect is predominant in the first mode.

Figure 9 compares the frequency for the subject-specific models in dependence of degree of cover anisotropy in the presence of a constant degree of heterogeneity $h = 4.00$ on one hand, and the frequency for the subject-specific models in dependence of degree of heterogeneity in the presence of a constant degree of cover anisotropy $\chi = 5.00$ on the other. Increasing muscular activation, or in our model, increasing heterogeneity leads to an increase in the predicted fundamental frequency. This is expected because increase in heterogeneity corresponds to increased stiffness in the body region. On the other hand increase in anisotropy decreases the frequency, owing to increase in compliance in the cover. Simultaneous increase in values of both parameters is thereby counteractive. We observe that the combined effect, however, works to a different degree on the subject-specific models compared to the M5R1 model. In both cases, the curves of frequency variation for the subject-specific models deviate from isolines of M5R1 models of constant lengths much faster than when cover anisotropy and heterogeneity were considered in isolation. In particular, for the first mode, the effect of varying heterogeneity, while keeping cover anisotropy fixed, is found to be larger than the reverse case (fixing heterogeneity and varying anisotropy). The percentage differences between the SS model and the other subject-specific models is of the same order as before. In particular, R0 differs by less than 2%, R1 by less than 10% and R2 by about 50%.

DISCUSSION

In this paper a framework to construct geometrical models from subject-specific data was presented. It was shown how geometrically abstracted models can be created using this framework in an automated process with the underlying mathematical equations presented in this paper. Human intervention might be required in successfully implementing the procedure, especially to overcome lack of information from image slices. The image-slice data used in this paper was obtained from a casting method used to determine subject-specific glottal geometry. This data is similar in resolution to that obtainable through modest MRI capabilities available currently that can achieve a resolution of the order of 1 mm[46,35,31]. The geometric models were further enriched to incorporate VF histology. Consistent

micromechanical laws were used to define tissue properties. Below we discuss the results obtained above in the context of creating a canonical model that satisfactorily resembles the response of the real VF. Therefore all comparisons are made with the the geometrically accurate model SS, and deviations from it are interpreted as degradation in performance and accuracy.

Irreconciliability of the M5 model

This paper indicates that the widely used M5 geometry is not an appropriate choice for a canonical model in continuum analysis. There are two possible reasons for this: difference in sub-glottal geometry and quasi-2D (extruded) geometry. The first reason is supported by our observation that the models R0 and R1 performed better than model R2. To investigate the validity of the second reason, a quasi-2D model M5R1 with a cross-section similar to the mid-coronal section of R1 was created. It was expected to perform better than a quasi-2D model with a R2/M5-like cross section. However, there was a marked increase in percentage error in this model compared to R1 in all cases. The M5R1 model had a satisfactorily accurate modal response only for the homogeneous isotropic VF case. As either heterogeneity and cover anisotropy approach realistic levels, the length of an M5R1 and the ap-extent of the geometrically accurate model of identical modal response essentially diverge. The divergence is exacerbated when heterogeneity and anisotropy are combined. Thereby, we expect quasi-2D models based on M5 geometry to be strongly disadvantageous for modeling. The situation is irreconciliable because VFs are excited through a fluid-dynamic loading by the glottal air flow. If an M5R1 model is constructed to have an identical modal response as a geometrically accurate model, the fluid-dynamic loading will have a characteristic length scale different from reality.

An alternate canonical model

In this paper various alternate canonical models were analyzed for continuum analysis, and our results help to rationalize a choice. The geometrically abstracted model R0 was constructed from only the mid-coronal section image and two other gross dimensions: ap-extent of glottal orifice, $H - 2w$, and outer tracheal wall diameter H. The mid-coronal image automatically provides the dimension d_g. The modal response of this model was found to be within 98% accuracy. Furthermore, when coupled to glottal air-flow models, the characteristic length scales of the model and flow remain identical. This model geometry is also advantageous from the point of view of data acquisition required to construct the model. By eliminating the need to obtain multiple MRI slices, and consequently a higher resolution and a high intensity magnetic field, a significant simplification is achieved. The procedure presented in this paper to construct the model R0 can therefore be used to develop subject-specific models that have faithful mechanical response.

We do not foresee much advantage in choosing model R1 over R0. The gross dimensions $H - 2w$, H, d_g and the thickness of the VF (inferior-superior dimension) are required to create this model. The first three can be determined from a superior view, as with a clinical instrument like laryngoscope. However we are not aware of any technique that can determine the depth *in-vivo* without employing an MRI or other imaging paradigm. Moreover, the accuracy drops to about 90% with this model. Use of this model needs to be justified with respect to the research context. On the other hand, use of

the model R2 is strongly discouraged. Even though this model requires data that can be acquired through a superior view only, obviating an imaging procedure, it is seriously disadvantaged due to it inaccuracy.

Models R0, R1 and R2 have a unique advantage over the quasi-2D model M5R1, in that it is perhaps possible to recalibrate the eigenmode results obtained from these models so that they match model SS. This is because the error in these models, however large, is consistently of positive sign. However the model M5R1, variously overpredicts or underpredicts the modal response, depending on tissue properties and the mode in consideration. Possible reasons are differences in effective boundary conditions at the anterior and posterior ends, and the difference in ap depth. In the quasi-2D model, the anterior and posterior ends are held rigid and the VF vibrates like a beam with clamped conditions on both sides.

In the subject-specific models however, the support is somewhat compliant in that there is a volume of solid that is free to deform. Furthermore, the material properties of this region are those of the cover and this might possibly make the support condition further compliant. To test this hypothesis, we created an M5R1 model of length $L = 16.0$ mm with body-cover partitioning as described before. Additionally, all elements lying within a width $w' = 1.50$ mm of the anterior and posterior ends were specified as having cover properties. The anisotropy and heterogeneity were set to $\chi = 5.00$ and $h = 4.00$ respectively. This model was expected to isolate the effects of end-condition compliance arising due to geometry only, and suppress those due to material properties. The effective length of this model $L' = L - 2w' = 13.0$ mm is close to that of subject-specific models (table 2, column 6). We compare this model to subject-specific models in figure 9. Indeed, this model performs better that the original M5R1 model with length $L = 12.0$ mm. However there are two disadvantages. Firstly, there is no significant improvement over model R1, except in the third mode. And secondly, the sense of deviation depends on the mode: positive and large for mode 1, and decreases thereon to become negative for mode 3. Therefore, we conclude that the geometry of the subject-specific models, in particular their non-extruded construction, plays a significant role in ensuring a uniform sense of deviation, and thereby their potential to be calibrated.

Tissue properties and histology

Our work shows that the effort made in accurately determining geometry must be seriously weighed in comparison to accurately determining the mechanical behaviour of the tissue. In this paper, the sensitivity of modal response to tissue properties was found to be significant even with a computational model adhering closely to a subject's VF geometry. The fidelity of such a model's modal response is therefore as ambiguous as the ambiguity in the knowledge of the subject VF's tissue properties. Efforts need to be made to develop procedures that can reliably measure in-vivo tissue properties. Noninvasive methods (e.g., using sonography[47]) to characterize the mechanical behavior are an attractive choice. In the present study a constant cover thickness was assumed and the sensitivity of modal response to this parameter was not examined. This is due to the fact that histology is currently unobtainable from MRI data. In Herrera et al. [48] ex-vivo ferret and canine larynges were examined under high-intensity magnetic field (11.7 T) to establish that histological distinctions between lamina propria, muscle, epithelial tissue can be achieved. We believe this is an important development,

and our results clearly are in need of input from research in this direction.

CONCLUSIONS

From the present study, four main conclusions can be drawn. Specifically, these concern:

1. the geometry representation framework,
2. the proper construction and choice of a canonical model,
3. the relevance of extruded geometry models, and
4. the role of tissue biomechanical properties.

The mathematical representation of the VF geometry described herein is demonstrated to be versatile. This representation technique naturally follows slice-by-slice imaging methods; an example data-set available in literature was assimilated with minimal post-processing. It allows typical geometric abstractions to be easily conceptualized; a widely-used geometry specification was completely described by the variables used in the representation. Furthermore, the technique is readily implemented using a scripting language (Python) to control model construction steps within a commercial software package (Abaqus/CAE). The tool presented in the paper could be considered as a planning tool in clinical applications, for example, when modifications to VFs are considered by phonosurgery procedures[49,50], or when tissue replacements are implanted[51,52,53]. The strength of the method lies in its ability to significantly shorten the distance between subject-specific geometry features and modeling of VF dynamics.

Regarding the proper construction of a canonical model, a succession of geometric abstractions were constructed that reduced a subject-specific geometry to a widely-used extruded geometry specification available in voice literature. The mechanical response of these models – characterized by the first three eigenfrequencies – was analysed in dependence of geometric abstraction, and in the presence of variation in tissue biomechanical properties. It was found that, except for the naïve biomechanical property consideration of isotropic homogeneous VF tissue, geometric abstractions could cause unrealistic deviations in model response, thereby making the model irrelevant. Considerations of model construction overhead and model accuracy were factored in to arrive at an optimal choice of the canonical model.

In the extreme case of the extruded geometry model, a calibration exercise remained inconclusive because the deviations in model response were inconsistent in their dependence on tissue property variation. Care was excercised to demonstrate that geometric abstraction was the source this discrepancy, which remained even after providing for a correction due to possible differences in tissue biomechanical properties at support locations. This underlined the difficulty in using this geometry to construct models with realistic response characteristics. Contact between VFs is another aspect of VF dynamics which is of considerable interest, and presents a further complication in modeling. While not addressed in the present study, the present results indicate a strong dependence of the VF behavior on geometry, thus contact is expected to further complicate the behavior. Thereby studies on modeling contact using extruded geometries should be carefully reviewed. Such investigations are under consideration.

The present study also shed light on aspects of numerical modeling that deserve focus. Although the capability of extracting geometric detail *in vivo* has realised significant development recently, and continues

to be advanced, the present study advocates a strong focus on research towards determination of tissue mechanical properties *in vivo*. It was demonstrated that even for moderately abstracted geometries, correcting for model response deviation is challenging when tissue properties are not known with sufficient accuracy.

ACKNOWLEDGEMENT

The authors wish to gratefully acknowledge the support provided by NIDCD Grant 5RA1DC008290-04.

References

1. Zheng X, Bielamowicz S, Luo H, Mittal R. A computational study of the effect of false vocal folds on glottal flow and vocal fold vibration during phonation. *Ann Biomed Eng*. 2009;37(3):625–642.
2. Zhang Z. Characteristics of phonation onset in a two-layer vocal fold model. *J Acoust Soc Am*. 2009;125(2):1091–1102.
3. Kelleher JE, Zhang K, Siegmund T, Chan RW. Spatially varying properties of the vocal ligament contribute to its eigenfrequency response. *J Mech Behav Biomed*. 2010;3:600–609.
4. Zhang K, Siegmund T, Chan RW. Modeling of the transient responses of the vocal fold lamina propria. *J Mech Behav Biomed*. 2009;2(1):93–104.
5. Kelleher JE, Siegmund T, Chan RW, Henslee EA. Optical measurements of vocal fold tensile properties: Implications for phonatory mechanics. *J Biomech*. 2011;44(9):1729–1734.
6. Chen LJ. Investigations of mechanical stresses within human vocal folds during phonation. Ph.D. thesis; Purdue University; 2009.
7. Tao C, Jiang JJ, Zhang Y. Simulation of vocal fold impact pressures with a self-oscillating finite-element model. *J Acoust Soc Am*. 2006;119(6):3987–3994.
8. Hunter E, Titze I, Alipour F. A three-dimensional model of vocal fold abduction/adduction. *J Acoust Soc Am*. 2004;115(4):1747–1759.
9. Spencer M, Mongeau L, Siegmund T. Experimental study of the self-oscillation of a model larynx by digital image correlation. *J Acoust Soc Am*. 2008;123(2):1089–1103.
10. Šidlof P, Švec JG, Horáček JJ, Veselý J, Klepáček I, Havlík R. Geometry of human vocal folds and glottal channel for mathematical and biomechanical modeling of voice production. *J Biomech*. 2008;41(5):985–995.
11. Castelijns JA, Doornbos J, Jr. BV, Vielvoye GJ, Bloem JL. MR imaging of the normal larynx. *J Comput Assist Tomogr*. 1985;9(5):919–925.
12. Ford CN, Unger JM, Zundel RS, Bless DM. Magnetic resonance imaging (MRI) assessment of vocal fold medialization surgery. *Laryngoscope*. 1995;105(5):498–504.
13. Sakai F, Gamsu G, Dillon WP, Lynch DA, Gilbert TJ. MR imaging of the larynx at 1.5 T. *J Comput Assist Tomogr*. 1990;14(1):60–71.
14. Pickup BA, Thomson SL. Flow-induced vibratory response of idealized versus magnetic resonance imaging-based synthetic vocal fold models. *J Acoust Soc Am*. 2010;128(3):124–129.
15. Thomson SL, Mongeau L, Frankel SH. Aerodynamic transfer of energy to the vocal folds. *J Acoust Soc Am*. 2005;118(3):1689–1700.
16. Suh J, Frankel SH. Numerical simulation of turbulence transition and sound radiation for flow through a rigid glottal model. *J Acoust Soc Am*. 2007;121(6):3728–3739.
17. Erath BD, Plesniak MW. The occurrence of the Coanda effect in pulsatile flow through static models of the human vocal folds. *J Acoust Soc Am*. 2006;120(2):1000–1011.
18. Scherer RC, Shinwari D, DeWitt KJ, Zhang C, Kucinschi BR, Afjeh AA. Intraglottal pressure profiles for a symmetric and oblique glottis with a divergence angle of 10 degrees. *J Acoust Soc Am*. 2001;109(4):1616–1630.
19. Ishizaka K, Flanagan JL. Synthesis of voiced sounds from a two-mass model of the vocal cords. *AT&T Tech J*. 1972;51(6):1233–1268.
20. Scherer RC, Titze IR, Curtis JF. Pressure-flow relationships in two models of the larynx having rectangular glottal shapes. *J Acoust Soc Am*. 1983;73(2):668–676.
21. van den Berg J, Zantema JT, Doornenball P. On the air resistance and the bernoulli effect of the human larynx. *J Acoust Soc Am*. 1957;29:626–631.
22. Gauffin J, Binh N, Ananthapadmanabha TV, Fant G. Glottal geometry and volume velocity waveform. In: Bless DM, Abbs JH, eds. *Vocal Fold Physiology*. Vocal fold physiology; Madison, WI: College-Hill Press; 1981:.
23. Horáček J, Anne-Maria L, Šidlof P, Murphy P, Švec JG. Comparison of accelaration and impact stress as possible loading factors in phonation: a computer modeling study. *Folia Phoniatr*

Logo. 2009;61(3):137–145.

24. Scherer RC, Shinwari D, DeWitt KJ, Zhang C, Kucinschi BR, Afjeh AA. Intraglottal pressure profiles for a symmetric and oblique glottis with a uniform duct (L). *J Acoust Soc Am*. 2002;112(4):1253–1256.
25. Michael H. Krane TW. Theoretical assessment of unsteady aerodynamic effects in phonation. *J Acoust Soc Am*. 2006;120(3):1578–1588.
26. Erath BD, Plesniak MW. An investigation of asymmetric flow features in a scaled-up driven model of the human vocal folds. *Exp Fluids*. 2010;49(1):131–146.
27. Triep M, Brücker C, Schröder W. High-speed PIV measurements of the flow downstream of a dynamic mechanical model of the human vocal folds. *Exp Fluids*. 2005;39(2):232–245.
28. Alipour F, Berry DA, Titze IR. A finite-element model of vocal-fold vibration. *J Acoust Soc Am*. 2000;108(6):3003–3012.
29. de Oliveira Rosa M, Pereira JC, Grellet M, Alwan A. A contribution to simulating a three-dimensional larynx model using the finite-element model. *J Acoust Soc Am*. 2003;114(5):2893–2905.
30. Gunter H. A mechanical model of vocal fold collision with high spatial and temporal resolution. *J Acoust Soc Am*. 2003;113(2):994–1000.
31. Rubin JS, Summers P, Harris T. Visualization of the human larynx: a three-dimensional computer modeling tool. *Auris Nasus Larynx*. 1998;25(3):303–308.
32. Kikinis R, Wolfensberger M, Boesch C, Martin E. Larynx: MR imaging at 2.35 T. *Radiology*. 1989;171:165–169.
33. Zhang Z, Neubauer J, Berry DA. Physical mechanisms of phonation onset: A linear stability analysis of an aeroelastic continuum model of phonation. *J Acoust Soc Am*. 2007;122(4):2279–2295.
34. Farley GR. A biomechanical laryngeal model of voice f0 and glottal width control. *J Acoust Soc Am*. 1996;100(6):3794–3812.
35. Selbie WS, Gewalt SL, Ludlow CL. Developing an anatomical model of the human laryngeal cartilages from magnetic resonance imaging. *J Acoust Soc Am*. 2002;112(3, Part 1):1077–1090.
36. Hirano M, Kurita S, Yukizane K, Hibi S. Asymmetry of the laryngeal framework: A morphologic study of cadaver larynges. *Ann Otol Rhinol Laryngol*. 1989;98:135–140.
37. Cook DD, Mongeau L. Sensitivity of a continuum vocal fold model to geometric parameters, constraints, and boundary conditions. *J Acoust Soc Am*. 2007;121(4):2247–2253.
38. Tao C, Jiang JJ, Zhang Y. A fluid-saturated poroelastic model of the vocal folds with hydrated tissue. *J Biomech*. 2009;42(6):774–780.
39. Hirano M. Structure and vibratory behavior of the vocal folds. In: Sawashima M, Cooper FM, eds. *Dynamic aspects of speech production*. University of Tokyo Press; 1977:.
40. Hirano M, Kurita S, Nakashima T. The structure of the vocal folds. In: Stevens KN, Hirano M, eds. *Vocal fold physiology*. University of Tokyo Press; 1981:33–41.
41. Titze I. The myoelastic aerodynamic theory of phonation. Iowa City, Iowa: NCVS; 2006.
42. Daniel IM, Ishai O. Engineering mechanics of composite materials. 1st ed.; New York: Oxford University Press; 1994.
43. Oestreicher HL. Field and impedance of an oscillating sphere in a viscoelastic medium with an application to biophysics. *J Acoust Soc Am*. 1951;23(6):707–714.
44. Alipour-Haghighi F, Titze IR. Viscoelastic modeling of canine vocalis muscle in relaxation. *J Acoust Soc Am*. 1985;78(6):1939–1943.
45. Hast MM. Mechanical properties of the vocal fold muscle. *Pract Oto-Rhino-Laryngol*. 1967;33:209–214.
46. Hu A, Wilson T, Ladak H, Haase P, Fung K. Three-dimensional educational computer model of the larynx: voicing a new direction. *Arch Otolaryngol*. 2009;135(7):677–681.
47. Tsai CG, Hsiao TY, Shau YW. Vocal fold wave velocity in the cover and body layers measured in vivo using dynamic sonography (oral). In: *Proceedings of the 7th International Conference on Advances in Quantitative Laryngology, Voice and Speech Research*. 2006:Groningen, the Netherlands.
48. Herrera VLM, Viereck JC, Lopez-Guerra G, Kumai Y, Kobler J, Karajanagi S, Park H, Hillman R, Zeitels SM. 11.7 Tesla magnetic resonance microimaging of laryngeal tissue architecture. *Laryngoscope*. 2009;119(11):2187–2194.
49. Remacle M, Friedrich G, Dikkers F, de Jong F. Phonosurgery of the vocal folds: a classification proposal. *Eur Arch Oto-Rhino-laryngol*. 2003;260(1):1–6.
50. Isshiki N, Morita H, Okamura H, Hiramoto M. Thyroplasty as a new phonosurgical technique. *Acta Otolaryng*. 1974;.
51. Tsunoda K, Kondou K, Kaga K, Niimi S, Baer T, Nishiyama K, Hirose H. Autologous transplantation of fascia into the vocal fold: long-term result of type-1 transplantation and the future. *Laryngoscope*. 2005;115:1–10.

52. Chhetri DK, Head C, Revazova E, Hart S, Bhuta S, Berke GS. Lamina propria replacement therapy with cultured autologous fibroblasts for vocal folds scars. *Otolaryngology – Head and Neck Surgery*. 2004;131(6):864–870.
53. Duflo S, Thibeault SL, Li W, Shu XZ, Prestwich GD. Vocal fold tissue repair in vivo using a synthetic extracellular matrix. *Tissue Engineering*. 2006;12(8):2171–2180.
54. Gray H. Anatomy of the human body. 20th ed.; Philadelphia: Lea & Febiger; 1918.

Variables (Roman)

a: hyperellipse semi-minor axis

b: hyperellipse semi-minor axis

B: M5 model parameter

C: distance from center

d_g: glottal gap

D: depth

E: elastic modulus

f_j: frequency of j-th mode

G: bulk modulus

h: heterogeneity parameter

H: tracheal wall diameter

k: hyperellipse curvature parameter

L: length

L': effective length

L_{elem}: global element edge length

M: number of planes

N: number of closed curves

P: point

$\bar{P}$: point

Q_1, Q_2, Q_3, Q_4, Q_5: M5 model parameters

R: radius

R_0, R_ψ, R_L, R_{40}: M5 model parameters

S_j: curve j

t: cover thickness

T: M5 model parameter

V: volume

w: width at ant-pos ends

w': length reduction at ends

x: cartesian coordinate of point P

$\bar{x}$: cartesian coordinate of point $\bar{P}$

Variables (Greek)

∂C: shell

ϕ: eigenvector

ν: Poisson's ratio

ρ: density

ψ: glottal angle

ω: eigenfrequency

χ: degree of anisotropy

Abbreviations

2D: two-dimensional

3D: three-dimensional

ap: anterior–posterior

CAD: computer-aided design

CC: cricoid cartilage

CT: computed tomography

FE: finite element

is: inferior–superior

ml: medial–lateral

MR(I): magnetic resonance (imaging)

VF: vocal fold

Superscripts

i: index

M: dimension

N: dimension

Subscripts

ap: anterior–posterior

b: body

c: cover

Table 1: Glossary

Variables (Roman)

$x_{\min}$, $x_{\max}$: extrema

y: cartesian coordinate of point P

$\bar{y}$: cartesian coordinate of point $\bar{P}$

z: cartesian coordinate of point P

$\bar{z}$: cartesian coordinate of point $\bar{P}$

$\mathbb{K}$: stiffness matrix

$\mathbb{M}$: mass matrix

M5, M5R1, R0, R1, R2, SS: model names

$\mathcal{G}$: surface

$\mathcal{T}$: surface

Subscripts (contd.)

f: fiber

is: inferior–superior

j: index

L: left

m: matrix

ml: medial–lateral

R: right

Table 1: Glossary (contd.)

Model	H [mm]	w [mm]	R [mm]	C [mm]	$H-2w$ [mm]	# elements
SS	18.0	3.10	35.5	17.5	11.9	321 368
R0	17.4	1.60	35.2	17.8	14.2	215 994
R1	15.5	1.40	35.4	19.9	12.7	124 478
R2	15.5	1.40	35.4	19.9	12.7	173 635
$\langle q \rangle$	16.6	1.88	35.4	18.8	12.9	–
$\frac{\max[q-\langle q \rangle]}{\langle H \rangle}$	–	0.0735	0.0120	0.0783	0.0783	–

Table 2: Geometry parameter values and total number of elements for the models considered. Also indicated are deviations in geometry parameters across models. For a parameter q, its average value is denoted by $\langle q \rangle$.

	Case I	Case II	Case III	Case IV
χ	1.00	2.00	5.00	10.0
$E_{c,ap}$ [kPa]	6.00	6.00	6.00	6.00
$E_{c,ml}$ [kPa]	6.00	3.00	1.20	0.600
$G_{c,ml-is}$ [kPa]	2.07	2.23	2.28	2.29
$G_{c,ml-ap}$ [kPa]	2.07	1.02	0.404	0.202
$\nu_{c,ml-is}$	0.450	0.740	0.886	0.933
$\nu_{c,ml-ap}$	0.450	0.217	0.0866	0.0433

Table 3: Elastic constants of body and cover for various level of anisotropy.

Model	f_1 (Hz)	f_2 (Hz)	f_3 (Hz)
SS	71.5 (71.5, 71.5)	97.0 (96.1, 97.9)	105 (104, 106)
R0	70.7 (70.6, 70.7)	95.4 (95.3, 95.6)	104 (103, 105)
R1	75.7 (75.7, 75.7)	107 (106, 107)	112 (111, 113)
R2	73.0 (72.9, 73.0)	105 (104, 105)	114 (112, 115)

Table 4: Predicted eigenfrequencies for homogeneous isotropic vocal fold models.

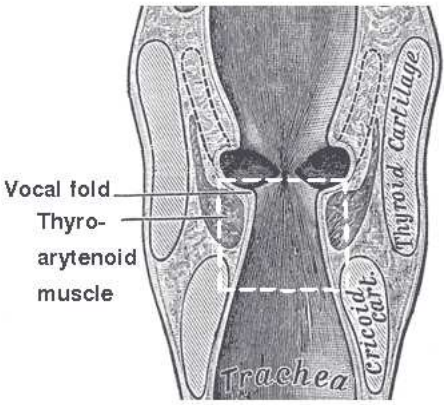

Figure 1: Schematic of the vocal folds, underlying muscles and surrounding hard tissues as seen at a coronal section (adapted from Gray [54]). White dashed lines depict the boundary of the system considered in this paper.

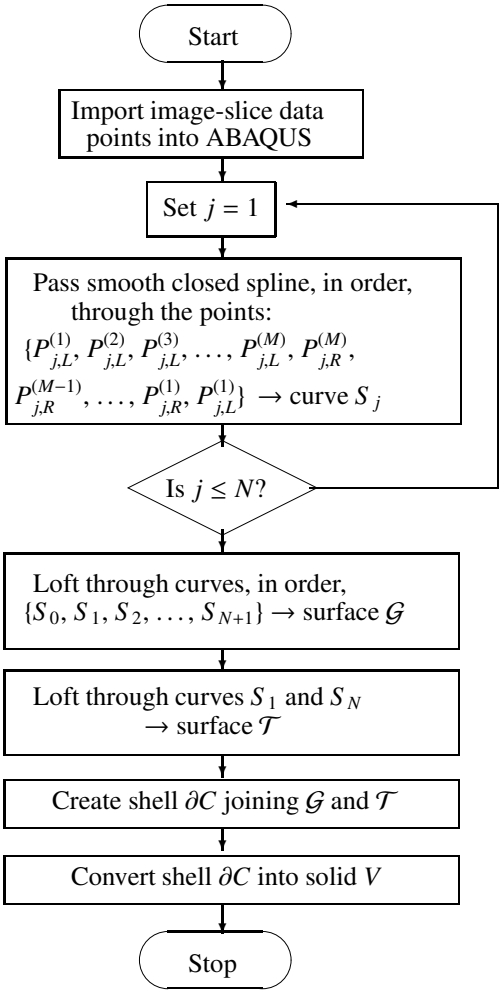

Figure 2: Flowchart for the process of creating 3D continuum models of vocal fold using image-slice data.

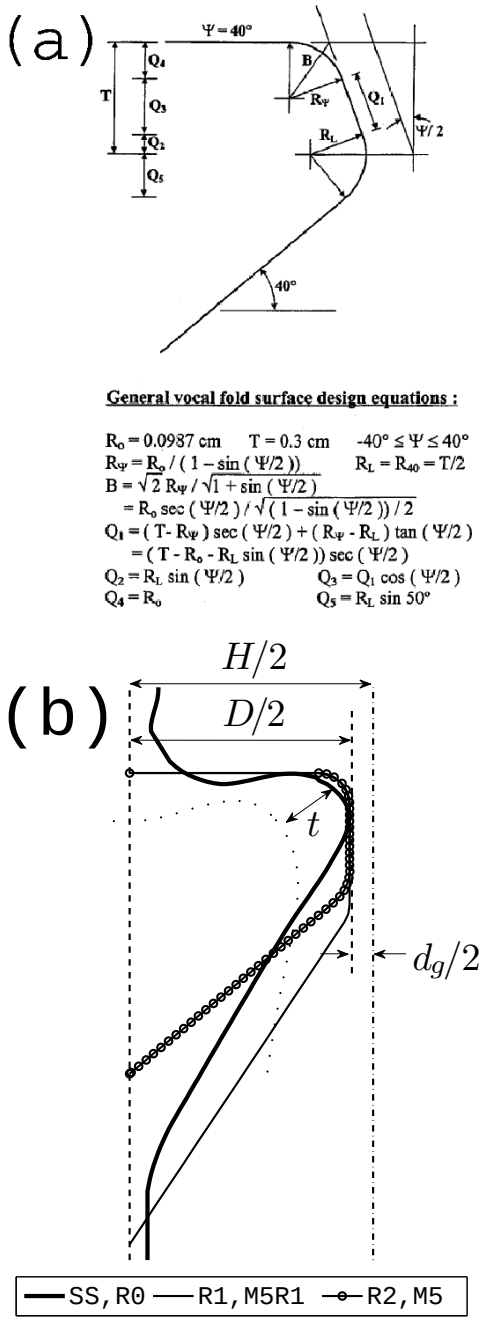

Figure 3: (a) The M5 profile, with permission to reproduce from Scherer et al. [18] (b) Comparision of the M5 profile, $\psi = 0°$, and various mid-coronal sections used in this study. The dash-dotted line in (b) is the mid-saggital plane, at distances $d_g/2$ and $H/2$ from the medial edge of the mid-coronal section and from the outer tracheal wall respectively. The dotted curve is the interface between body and cover.

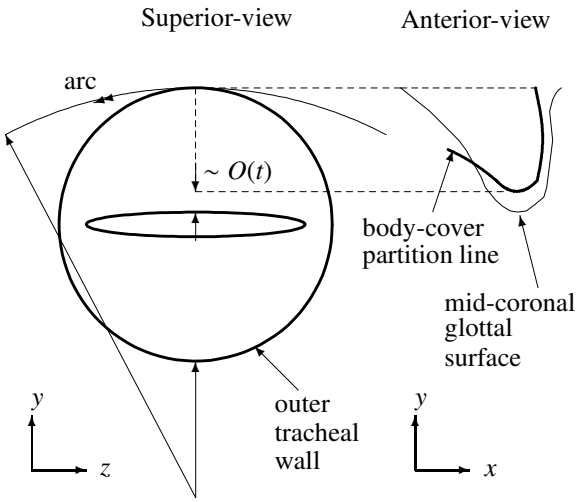

Figure 4: Partitioning the vocal fold volume into body and cover regions by sweeping a partition line along an arc.

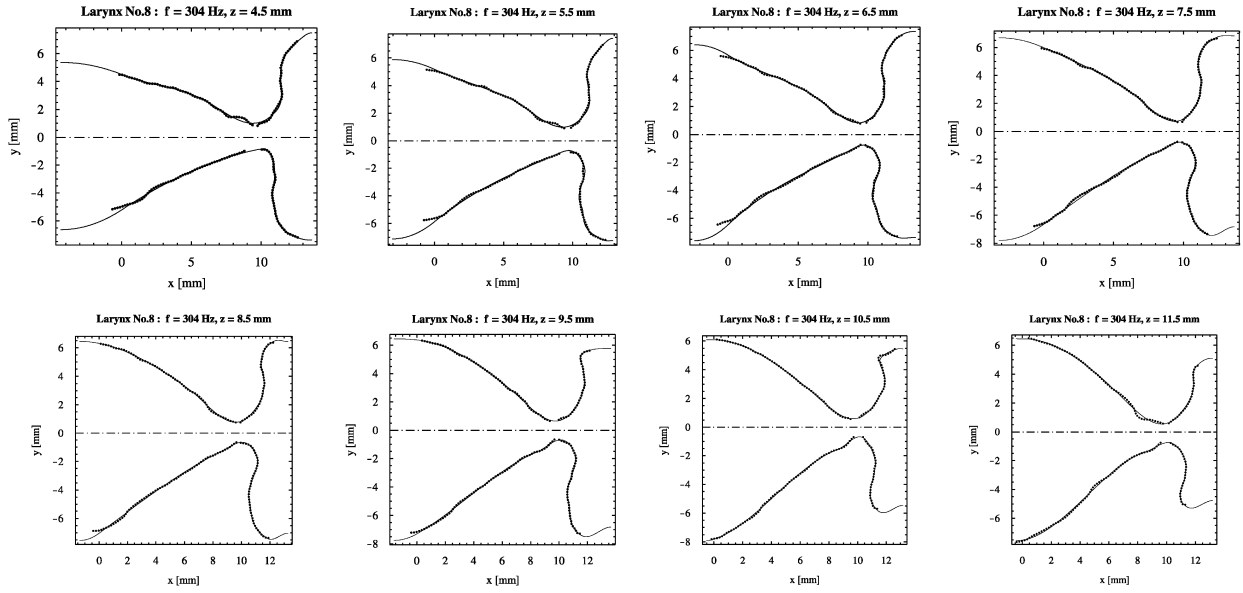

Figure 5: Image-slices for the vocal folds of 72-year old female subject (with permission from Šidlof et al. [10]).

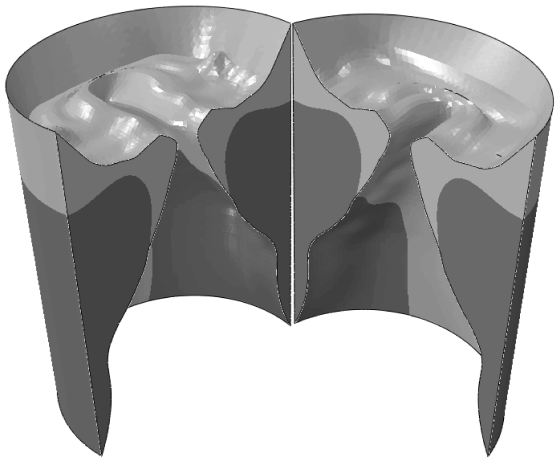

Figure 6: The two parts of model SS corresponding to slice made at z = 6.5 mm in figure 5 (top row, third from left). The body (dark) and cover (light) regions are colored differently.

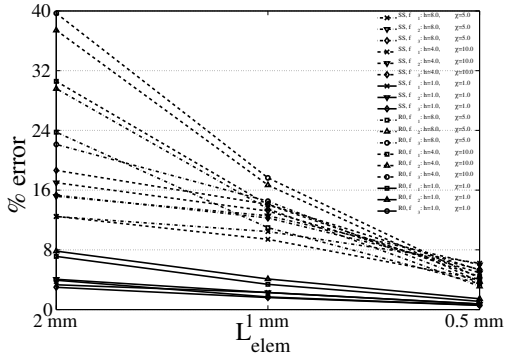

Figure 7: Mesh independence results for models SS and R0. The first three frequencies are considered. Percentage errors associated with meshes of global element edge length L_{elem} = 2.0 mm, 1.0 mm and 0.5 mm, with respect to a L_{elem} = 0.3 mm mesh are given for cases (h = 1.0, χ = 1.0), (h = 8.0, χ = 5.0) and (h = 4.0, χ = 10.0).

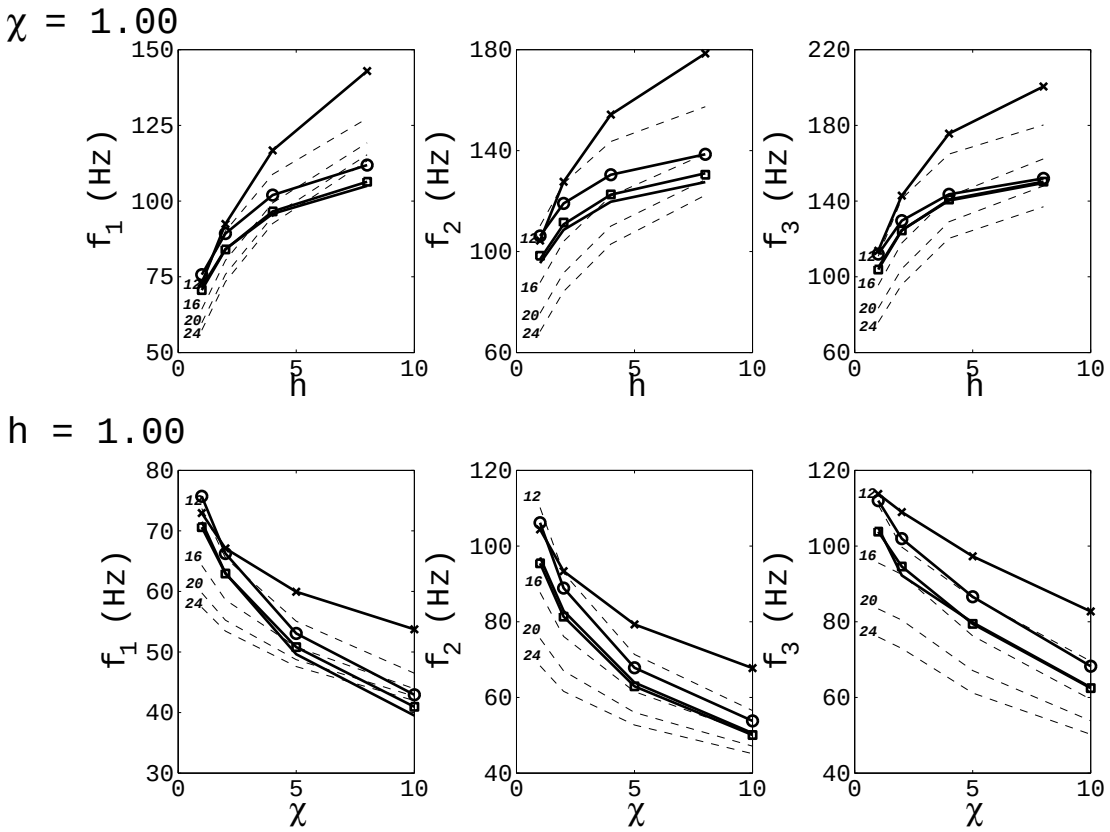

Figure 8: Predicted eigenfrequencies in dependence of heterogeneity (top) and anisotropy (bottom), considered in the absence of one another. SS, solid line without symbol; R0, squares (□); R1, circles (○); R2, crosses (×). Dashed lines correspond to M5R1 model. Numbers adjacent to the dashed lines indicate model length in millimeters.

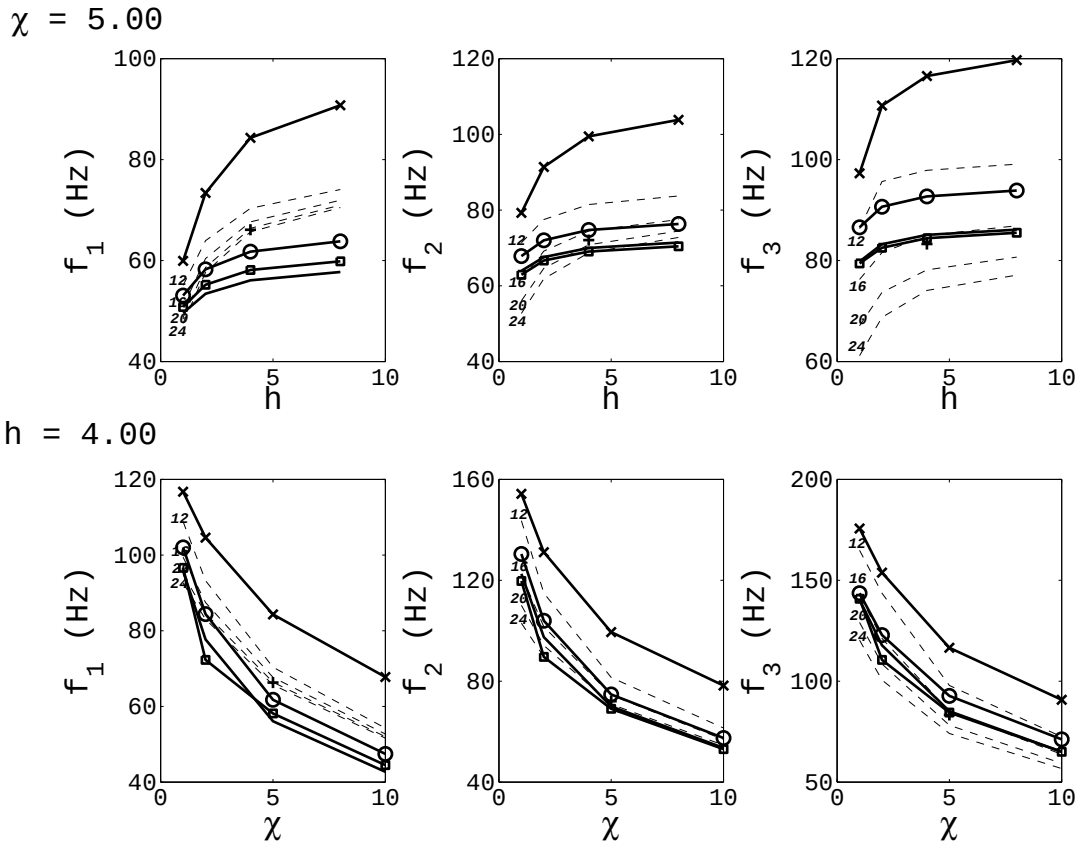

Figure 9: Predicted eigenfrequencies in dependence of heterogeneity (top) and anisotropy (bottom), considered in the presence of one another. SS, solid line without symbol; R0, squares (□); R1, circles (○); R2, crosses (×). Dashed lines correspond to M5R1 model. Numbers adjacent to the dashed lines indicate model length in millimeters. The plus symbol (+) corresponds to an M5R1 model with *ap*-ends constituting of cover material.